

Calculations for electron-impact excitation and ionization of beryllium

Oleg Zatsarinny^{1,*}, Klaus Bartschat^{1,†}, Dmitry V. Fursa^{2,‡} and Igor Bray^{2,§}

¹*Department of Physics and Astronomy, Drake University, Des Moines, Iowa, 50311, USA and*

²*Curtin Institute for Computation and Department of Physics, Astronomy and Medical Radiation Science, Curtin University, GPO Box U1987, Perth, WA 6845, Australia*

(Dated: October 20, 2018)

The B -spline R -matrix and the convergent close-coupling methods are used to study electron collisions with neutral beryllium over an energy range from threshold to 100 eV. Coupling to the target continuum significantly affects the results for transitions from the ground state, but to a lesser extent the strong transitions between excited states. Cross sections are presented for selected transitions between low-lying physical bound states of beryllium, as well as for elastic scattering, momentum transfer, and ionization. The present cross sections for transitions from the ground state from the two methods are in excellent agreement with each other, and also with other available results based on nonperturbative convergent pseudostate and time-dependent close-coupling models. The elastic cross section at low energies is dominated by a prominent shape resonance. The ionization from the $(2s2p)^3P$ and $(2s2p)^1P$ states strongly depends on the respective term. The current predictions represent an extensive set of electron scattering data for neutral beryllium, which should be sufficient for most modeling applications.

PACS numbers: 34.80.Bm, 34.80.Dp

I. INTRODUCTION

Beryllium is used as a surface material in the JET project [1] and for the plasma-facing walls in ITER [2]. This calls for accurate e-Be scattering data, as evidenced by recent Coordinated Research Projects and Technical Meetings organized on this topic by the International Atomic Energy Agency [3, 4]. Beryllium is among the most reactive elements, and its high chemical activity as well as its toxicity make it virtually impossible to obtain reliable values of the electron-impact cross sections from direct measurements with traditional setups.

Due to the lack of experimental data, researchers in plasma modeling currently have to rely entirely on theoretical predictions. For this reason, it is important to estimate the accuracy of the available theoretical data. Extensive calculations utilizing state-of-the-art computational methods, such as R -matrix with pseudostates (RMPS) [5, 6], convergent close-coupling (CCC) [7], and time-dependent close-coupling (TDCC) [8], were performed already more than a decade ago. All these calculations indicate a slow convergence of the close-coupling expansion for certain transitions and significant effects originating from coupling to the target continuum. Due to the importance of the e-Be collision system, the topic remains under active investigation, with the most recent CCC predictions published in 2015 [9].

The purpose of the present paper is to provide an extensive and complete (for most modeling applications) set of electron scattering data for neutral beryllium, includ-

ing elastic scattering, momentum transfer, excitation, and ionization from the ground state as well as a number of excited states, including the metastable $(2s2p)^3P$ state, which is of particular importance for collisional radiative models. The calculations reported below were carried out with the B -spline R -matrix (close-coupling) code [10]. As an independent check on these predictions, we also performed CCC calculations containing a large number of pseudostates in the close-coupling expansion. Good agreement between these independent calculations should provide additional confidence in the accuracy of the obtained cross sections while any discrepancy would allow to identify a possible source of a problem.

The distinct feature of the BSR approach is its ability to employ term-dependent nonorthogonal orbitals in the description of the target states. This allows us to optimize individual atomic wave functions independently and thereby generate an accurate description of the target states with relatively few configurations. Over the past decade, the BSR code (along with its relativistic extension, DBSR [11]) has been successfully applied to a number of targets, including those with multiple open shells [12]. Compared to some of those more complex systems, neutral beryllium is relatively simple, in particular if only single-electron excitations from the $2s^2$ filled outer subshell are considered. For practical applications, this simplicity offers the advantage of allowing for cross checks between the predictions from several highly sophisticated methods, as done with BSR and CCC calculations presented here, rather than having to rely on just a single approach.

In general, it is very helpful to investigate electron-atom collision systems with different computational approaches, particularly when high accuracy is required in applications. Previous examples include, but are not limited to, e-Be⁺ [13], e-Be²⁺ [14], and e-Li [15]. For quasi

*Electronic Address: oleg.zatsarinny@drake.edu

†Electronic Address: klaus.bartschat@drake.edu

‡Electronic Address: d.fursa@curtin.edu.au

§Electronic Address: i.bray@curtin.edu.au

two-electron targets, as considered here, the complexity of the electron-collision problem is such that substantial discrepancies may occur. This was recently highlighted for the e-Mg and e-Al⁺ collision systems [16].

The manuscript is organized as follows: After discussing the description of the target structure, we summarize the most important aspects of the collision calculations. This is followed by a presentation of the cross sections for the most important transitions, starting with elastic scattering from Be in its ground state. Comparison of the results from the present BSR and CCC calculations with those from previous RMPS calculations, as well as a systematic study of the effects of increasing channel coupling on the predictions, provides a basis for estimating the accuracy of the present dataset.

II. STRUCTURE CALCULATIONS

A. BSR

The target states of beryllium in the present calculations were generated by combining the multi-configuration Hartree-Fock (MCHF) and the B -spline box-based close-coupling methods [17]. We tried to account for the principal correlation effects, while bearing in mind that the final multi-configuration expansions still needed to be dealt with in the subsequent collision calculation with one more electron to be coupled in. Since relativistic effects are small in beryllium, certainly when it comes to their effect on electron collisions in practice, we used the nonrelativistic LS -coupling approximation, with the structure of the multi-channel target expansion chosen as

$$\begin{aligned} \Phi(2snl, LS) = & \sum_{nl} a_{nl}^{LS} \{\phi(2s)P(nl)\}^{LS} \\ & + \sum_{nl} b_{nl}^{LS} \{\phi(2p)P(nl)\}^{LS} \\ & + \sum_{l,l'} c_{ll'}^{LS} \varphi(2l2l')^{LS}. \end{aligned} \quad (1)$$

Here $P(nl)$ denotes the wave function of the outer valence electron, while the ϕ and φ functions stand for the configuration interaction (CI) expansions of the corresponding ionic and specific atomic states, respectively. These expansions were generated in separate MCHF calculations for each state using the MCHF program [18]. The expansion (1) can be considered as a model for the entire $2snl$ and $2pnl$ Rydberg series of the beryllium spectrum, including autoionizing states and continuum pseudostates.

The most correlated $2s^2$, $2s2p$ and $2p^2$ states require more accurate descriptions. These states were represented by separate MCHF expansions, with the orbitals specifically optimized for each given term. Although abbreviated as $\varphi(2l2l')^{LS}$ in Eq. (1), the particular expansions for these states include all single and double ex-

citations from the $2s$ and $2p$ orbitals to the $3l$ and $4l$ ($l = 0 - 3$) correlated orbitals.

A more extensive description of core-valence correlation would require additional ionic states by opening the $1s^2$ shell. Their inclusion, however, would have considerably increased the target expansions and made them no longer tractable in the subsequent scattering calculations.

The unknown functions $P(nl)$ for the outer valence electron were expanded in a B -spline basis, and the corresponding equations were solved subject to the condition that the wave functions vanish at the boundary. The B -spline coefficients for the valence orbitals $P(nl)$, along with the various expansion coefficients in (1), were obtained by diagonalizing the N -electron atomic hamiltonian. Since the B -spline bound-state close-coupling calculations generate different nonorthogonal sets of orbitals for each atomic state, their subsequent use is somewhat complicated. On the other hand, our configuration expansions for the atomic target states contained between 10 and 50 configurations for each state and hence could still be used in the collision calculations with the available computational resources.

The number of spectroscopic bound states that can be generated in the above scheme depends on the B -spline box radius. In the present calculations, the latter was set to $40 a_0$, where $a_0 = 0.529 \times 10^{-10}$ m is the Bohr radius. This allowed us to obtain accurate descriptions of the beryllium states with principal quantum number for the valence electron up to $n = 4$.

B. CCC

As for the BSR method, the nonrelativistic formulation of the CCC method was adopted. We describe the Be atom by a model of two valence electrons above a frozen Hartree-Fock ($1s^2$) core. This is the same approximation as in the present BSR calculations. The calculations of the Be target states start with the Hartree-Fock calculation for the Be⁺ ion, which allows us to obtain the $1s$ core orbital. The quasi one-electron Hartree-Fock hamiltonian of the Be⁺ ion is then diagonalized in a basis of Laguerre functions. We add a one-electron polarization potential to the Be⁺ hamiltonian to improve the agreement of the Be⁺ energy levels with the corresponding experimental values. The number of Laguerre functions is $N_l = 18 - l$, and the exponential fall-offs were chosen as $\lambda_l = 0.9$ with the angular momentum ranging from $l = 0$ to $l = 3$. The result of the diagonalization are one-electron (pseudo) states of the Be⁺ ion. In the present calculations we drop the two highest-lying Be⁺ states, as they lead to high-energy Be states that are always closed at the energies considered in the present work.

The one-electron basis is then used to expand the wave function of the Be atom in a set of antisymmetric two-electron configurations. We include all configurations of the type $\{2s, nl\}$ and $\{2p, nl\}$. In addition we include

TABLE I: Binding energies (in eV) for the spectroscopic target states included in the BSR and CCC expansions.

State	Term	BSR	CCC	NIST [19]
$2s^2$	1S	-9.287	-9.312	-9.323
$2s2p$	$^3P^o$	-6.564	-6.601	-6.598
$2s2p$	$^1P^o$	-4.000	-3.952	-4.045
$2s3s$	3S	-2.854	-2.860	-2.865
$2s3s$	1S	-2.518	-2.539	-2.544
$2p^2$	1D	-2.240	-2.238	-2.270
$2s3p$	$^3P^o$	-2.004	-2.014	-2.019
$2p^2$	3P	-1.853	-1.811	-1.922
$2s3p$	$^1P^o$	-1.836	-1.838	-1.860
$2s3d$	3D	-1.623	-1.625	-1.629
$2s3d$	1D	-1.314	-1.314	-1.335
$2s4s$	3S	-1.321	-1.324	-1.325
$2s4s$	1S	-1.222	-1.230	-1.233
$2s4p$	$^3P^o$	-1.031	-1.036	-1.039
$2s4p$	$^1P^o$	-0.999	-1.004	-1.011
$2s4d$	3D	-0.896	-0.895	-0.899
$2s4f$	$^3F^o$	-0.857	-0.856	-0.862
$2s4f$	$^1F^o$	-0.857	-0.856	-0.862
$2s4d$	1D	-0.779	-0.777	-0.795
$2s5s$	3S	-0.765	-0.742	-0.767
$2s5s$	1S	-0.723	-0.690	-0.728

$\{nl, n'l'\}$ configurations with $n, n' \leq 3$. This choice of configurations is practically the same as in (1). The latter configurations allow us to accurately account for the electron-electron correlations that are important for the ground state and the low-lying excited states of the Be atom. The former set of configurations provides a description of physical and pseudo excited states as well as a square-integrable representation of the target continuum. This set of configurations is used to diagonalize the quasi two-electron hamiltonian of Be and thereby obtain the set of Be target states used in the scattering calculations. We include a two-electron polarization potential to further improve the description of the ground state and the low-lying excited states. These one- and two-electron polarization potentials are employed in the CCC calculations but are not adopted in the BSR model. In practice, however, the polarization potentials lead to only minor changes in the target wave functions.

C. Energy Levels and Oscillator Strengths

Table I compares the calculated spectrum of beryllium with the values recommended by NIST [19] for various multiplets included in the scattering calculations described below. Details of the evaluation procedure of the available data at the time of the original critical assessment were given by Kramida and Martin [20], where the original sources can also be found. References to more recent work, almost all theoretical, are also available from the NIST website. The overall agreement between experiment and our theories is very satisfactory, in

particular in light of the fact that our structure descriptions are meant for the subsequent collision calculation, rather than as structure models on their own. In the BSR model, specifically, the deviations from the NIST-recommended values in the energy splitting are less than 45 meV for most states, with a few larger ones (up to 69 meV) seen only for the $2p^2$ states. In the final BSR scattering calculations, we slightly adjusted the hamiltonian matrix elements, which allowed us to use the experimental target energies.

In the CCC model, the exponential fall-offs of the Laguerre basis were chosen in such a way that the target states of Be are well described up to principal quantum number $n = 4$. These states were referred to as the spectroscopic bound states in the BSR structure calculations above. As seen from Table I, the accuracy of the CCC target states is of the same level as for the target states obtained in the BSR calculations. This is particularly pleasing given the different underlying one-electron basis orbitals in the two methods.

The quality of our target descriptions can be further assessed by comparing the results for the oscillator strengths of various transitions with experimental data and other theoretical predictions. Accurate oscillator strengths are very important to obtain reliable absolute values for the excitation cross sections, especially for optically allowed transitions at high incident electron energies. A comparison of our oscillator strengths is given in Table II with the recommended data from the NIST compilation [19]. The latter recommendations are based on the semirelativistic Breit-Pauli calculations by Tachiev and Froese Fischer [21]. The f -values for the fine-structure transitions were converted to the corresponding multiplet LS -values. We see good agreement for all these transitions. Table II also contains the ratio of theoretical oscillator strengths obtained in the length and velocity forms of the electric dipole operator. This ratio can, to some extent, be considered an accuracy indicator for the calculated f -values. For most transitions, the length (f_L) and velocity (f_V) values agree within a few percent, and once again the quality of the BSR and CCC results is comparable.

III. COLLISION CALCULATIONS

A. BSR

The close-coupling expansion in our most extensive model contained 660 states of neutral beryllium, with 29 states representing the bound spectrum and the remaining 631 the target continuum corresponding to ionization of the $2s^2$ subshell. We included all singlet and quartet target states of configurations $2snl$ and $2pnl$ with orbital angular momentum $l = 0 - 3$ for the outer electron and total orbital angular momenta $L = 0 - 4$. The continuum pseudostates in the present calculations cover the energy region up to 60 eV above the ionization limit. This

TABLE II: Comparison of oscillator strengths in Be: BSR and CCC models.

lower level	upper level	BSR		CCC		NIST [19]
		f_L	$\Delta[\%]^a$	f_L	$\Delta[\%]^a$	
$2s^2 \ ^1S$	$2s2p \ ^1P^\circ$	1.36	4.3	1.39	5.7	1.37
	$2s3p \ ^1P^\circ$	1.32E-02	10.1	1.5E-02	27	8.98E-3
	$2s4p \ ^1P^\circ$	2.68E-04	20.8	9E-6	-	-
$2s2p \ ^3P^\circ$	$2s3s \ ^3S$	8.29E-02	4.4	8.16E-02	6.8	8.44E-2
	$2p^2 \ ^3P$	4.55E-01	5.5	4.57E-01	2.1	4.47E-1
	$2s3d \ ^3D$	2.94E-01	1.3	2.91E-01	1.0	2.99E-1
	$2s4s \ ^3S$	1.17E-02	5.0	1.15E-02	10.0	1.18E-2
	$2s4d \ ^3D$	1.01E-01	1.5	9.76E-02	1.0	9.61E-2
$2s2p \ ^1P^\circ$	$2s3s \ ^1S$	1.18E-01	5.7	1.22E-01	0.5	1.15E-1
	$2p^2 \ ^1D$	1.36E-03	12.0	1.99E-03	55	-
	$2s3d \ ^1D$	3.94E-01	1.3	3.95E-01	2.0	3.98E-1
	$2s4s \ ^1S$	8.53E-03	9.4	8.85E-03	2.2	9.81E-3
	$2s4d \ ^1D$	2.00E-01	0.5	1.91E-01	1.3	1.77E-1
$2s3s \ ^3S$	$2s3p \ ^3P^\circ$	1.14	5.3	1.13	3.0	1.13
	$2s4p \ ^3P^\circ$	4.40E-03	35.9	3.36E-03	27.0	3.51E-3
$2s3s \ ^1S$	$2s3p \ ^1P^\circ$	9.79E-01	8.3	9.73E-01	1.3	9.57E-1
	$2s4p \ ^1P^\circ$	8.53E-03	38.9	7.82E-03	16.0	9.68E-3
$2p^2 \ ^1D$	$2s3p \ ^1P^\circ$	7.13E-02	9.6	7.09E-02	14	-
	$2s4p \ ^1P^\circ$	4.86E-03	12.1	4.61E-03	25	-
	$2s4f \ ^1F^\circ$	1.61E-01	2.7	1.60E-01	1.9	1.56E-1
$2s3p \ ^3P^\circ$	$2s3d \ ^3D$	4.98E-01	0.4	5.04E-01	0.5	-
	$2s4s \ ^3S$	2.19E-01	4.3	2.16E-01	3.2	2.18E-1
	$2s4d \ ^3D$	1.42E-01	0.4	1.34E-01	0.2	1.33E-1
$2s3p \ ^1P^\circ$	$2s3d \ ^1D$	6.99E-01	3.7	6.93E-01	3.2	6.78E-1
	$2s4s \ ^1S$	2.11E-01	6.3	2.14E-01	2.0	-
	$2s4d \ ^1D$	1.92E-02	13.0	1.74E-02	9.2	1.74E-2
$2s3d \ ^3D$	$2s4p \ ^3P^\circ$	8.17E-02	0.3	8.25E-02	0.6	8.09E-2
	$2s4f \ ^3F^\circ$	8.90E-01	3.0	8.75E-01	2.6	8.74E-1
$2s4s \ ^3S$	$2s4p \ ^3P^\circ$	1.63	2.8	1.62	2.2	-
$2s3d \ ^1D$	$2s4p \ ^1P^\circ$	2.06	4.6	2.06	5.0	-
	$2s4f \ ^1F^\circ$	1.03	2.9	1.02	3.4	1.02
$2s4s \ ^1S$	$2s4p \ ^1P^\circ$	1.45	5.0	1.45	2.0	-
$2s4p \ ^3P^\circ$	$2s4d \ ^3D$	7.88E-01	0.3	8.08E-01	0.0	-
$2s4p \ ^1P^\circ$	$2s4d \ ^1D$	1.21	2.4	1.21	1.7	-
$2s4d \ ^3D$	$2s4f \ ^3F^\circ$	1.33E-01	4.6	1.46E-01	3.5	-
$2s4f \ ^1F^\circ$	$2s4d \ ^1D$	1.51E-01	6.3	1.46E-01	7.3	-

^a Percentage difference between the f_L and f_V values.

model will be referred to as BSR-660 below. Other time-independent close-coupling models will be labeled similarly by indicating the approach (RMPS, CCC, BSR), followed by the number of states included in the expansion.

The close-coupling equations were solved by means of the R -matrix method, using a parallelized version of the BSR code [10]. The distinctive feature of the method is the use of B -splines as a universal basis to represent the scattering orbitals in the inner region of $r \leq a$. Hence, the R -matrix expansion in this region takes the form

$$\Psi_k(x_1, \dots, x_{N+1}) = \mathcal{A} \sum_{ij} \bar{\Phi}_i(x_1, \dots, x_N; \hat{\mathbf{r}}_{N+1} \sigma_{N+1}) r_{N+1}^{-1} B_j(r_{N+1}) a_{ijk} + \sum_i \chi_i(x_1, \dots, x_{N+1}) b_{ik}. \quad (2)$$

Here the $\bar{\Phi}_i$ denote the channel functions constructed from the N -electron target states, while the splines $B_j(r)$ represent the continuum orbitals. The χ_i are additional $(N+1)$ -electron bound states. In standard R -matrix calculations [22], the latter are included one configuration at a time to ensure completeness of the total trial wave function and to compensate for orthogonality constraints imposed on the continuum orbitals. The use of nonorthogonal one-electron radial functions in the BSR method, on the other hand, allows us to completely avoid these configurations for compensating orthogonality restrictions. Sometimes, explicit bound channels in BSR calculations are used for a more accurate description of the true bound states in the collision system. In the present calculations, however, we did not employ any $(N+1)$ -electron correlation configurations in the expansion (2).

The B -spline basis in the present calculations contained 80 splines of order 8, with the maximum interval in this grid of $0.65 a_0$. This is sufficient for a good representation of the scattering electron wave functions for energies up to 150 eV. The BSR-660 collision model contained up to 1,566 scattering channels, leading to generalized eigenvalue problems with matrix dimensions up to 100,000 in the B -spline basis. Explicit numerical calculations were performed for partial waves with total orbital angular momenta $L \leq 25$. Taking into account the total spin and parity leads to 104 partial waves overall. A top-up procedure based on the geometric-series approximation was used to estimate the contribution from higher L values if needed. The calculation for the external region was performed using a parallelized version of the STGF program [23].

B. CCC

All states obtained from the diagonalization of the Be hamiltonian were included in the close-coupling expansion of the total wave function. Since the total number

of target states is 409, the corresponding calculations will be referred to as CCC-409. This model includes singlet and triplet states of positive and negative parity with total orbital angular momentum $L = 0 - 4$. Similarly to the BSR-660 model, the number of negative energy states is 29 and the remaining states are positive energy pseudostates modeling the target continuum. The positive-energy pseudostates span the energy region up to 130 eV for S -states, 120 eV for P -states, 100 eV for D -states, 80 eV for F -states, and 70 eV for G -states. While the negative-energy states in the BSR-660 and CCC-409 models are practically the same, the distribution of the positive energy pseudostates is very different. The use of the Laguerre basis in the CCC method leads to an exponential distribution of the states with energy that has a larger density of states at small energies. The B -spline basis, on the other hand, leads to a uniform distribution of the states with energy. This requires a larger number of states to cover approximately the same energy region.

In the CCC method the close-coupling expansion of the total wave function is inserted into the Schrödinger equation, which is transformed into momentum space, where it results in a set of coupled Lippmann-Schwinger equations for the T -matrix that is solved by standard techniques. The largest number of channels in the CCC-409 calculations was about 1,000 and the solution method required solving a set of linear equations of dimension up to 90,000 for each incident electron energy. The solution was obtained via a massively parallel hybrid OpenMP-MPI implementation that is standard for the entire suite of CCC programs (including the relativistic [24] and molecular [25] formulations). The calculations in the CCC-409 model were performed for partial waves up to the total orbital angular momentum $L = 15$. We then used an analytical Born subtraction technique to account for larger partial waves (formally up to infinity). To verify the accuracy of the analytical Born-subtraction technique, we performed calculations up to $L = 25$ at a number of energies and found negligible variations.

IV. RESULTS AND DISCUSSION

A. Elastic Scattering

Results for the elastic cross section for electron scattering from the beryllium in its ground state are presented in Fig. 1, where we compare the predictions from several BSR calculations to illustrate the convergence with the number of states included in the close-coupling expansion. As seen in the figure, the low-energy regime is dominated by a shape resonance, for which the convergence of the theoretical predictions is very slow. This is important but ultimately not surprising, since the very same effect was seen in e-Mg scattering [26]. As expected, the CCC-409 predictions are in good agreement with those from the BSR-660 model.

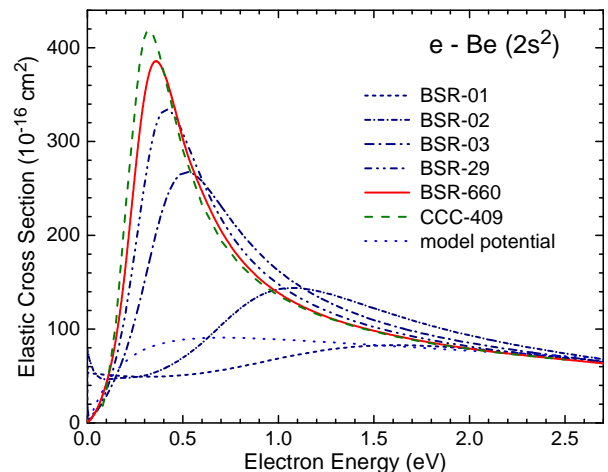


FIG. 1: (Color online) Cross sections for elastic electron scattering from beryllium atoms in their $(2s^2)^1S$ ground state at low energies in the region of the shape resonance. We present several BSR calculations to illustrate the convergence pattern. Also shown are the model-potential calculations by Reid and Wadehra [27].

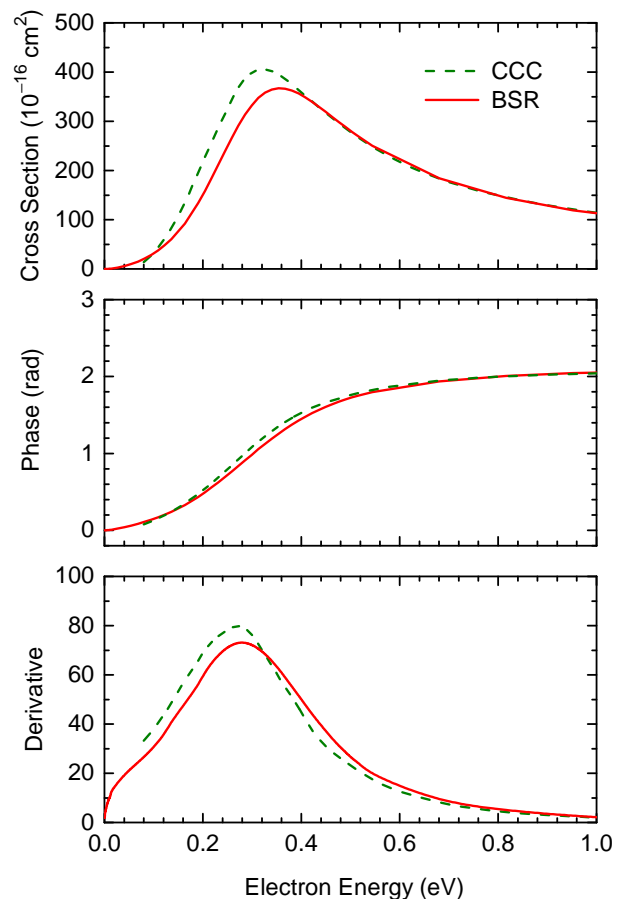


FIG. 2: (Color online) Cross sections, phase shift, and its derivative for the P partial wave for elastic electron scattering from beryllium atoms in the region of the shape resonance, as obtained in the BSR-600 and CCC-409 models.

The above shape resonance in elastic e-Be scattering has been the subject of numerous calculations with different methods. An overview of the many predictions is given in Table III of [28]. The results differ considerably, ranging for positions from 0.1 eV to 1.2 eV and widths from 0.14 eV to 1.78 eV, respectively. In this respect, it is worthwhile to provide the resonance parameters from direct scattering calculations.

The standard determination of such resonance parameters from collision calculations is based on the analysis of the phase shift in the corresponding partial wave. In the vicinity of a resonance, the phase shift δ behaves as

$$\delta(E) = \delta^0(E) + \tan^{-1} \frac{\Gamma/2}{E_r - E}. \quad (3)$$

Assuming that the background phase shift $\delta^0(E)$ is a smooth function of energy, the resonance width Γ is determined from the inverse of the energy derivative of the phase shift δ at the resonance energy E_r via

$$\Gamma = 2 \left[\frac{d\delta}{dE} \right]_{E=E_r}^{-1}. \quad (4)$$

Such an analysis for the P partial wave is given in Fig. 2, and the corresponding resonance parameters are listed in Table III.

TABLE III: Position (E) and width (Γ) of the shape resonance (in eV).

Method	cross section maximum		phase analysis	
	E_r	Γ	E_r	Γ
BSR	0.354	0.461	0.284	0.372
CCC	0.320	0.434	0.269	0.341

We note, however, that this procedure is somewhat ambiguous in the present case. Since the resonance is very wide and located close to the elastic threshold, the energy dependence of the phase shift given in Eq. (3) is disturbed. As a result, the phase shift increases by less than π radians as the energy passes through the resonance.

Another possibility, although not unique either, is to define the resonance parameters from the analysis of the relevant partial-wave (here the P -wave) cross section. An estimate for the resonance energy is then obtained from the maximum of the cross section while the (full) width is determined from half the height of this maximum. Table III also presents the resonance parameters generated in this way. The difference between the BSR and CCC predictions, and the difference between the values obtained in the two ways of analyzing the results, provide an indication of the likely uncertainty of the resonance parameters in the present calculations. Taking the averages of the results obtained in the schemes outlined above, we estimate the position at about $0.31 \text{ eV} \pm 0.04 \text{ eV}$ above the elastic threshold with a width of $0.40 \text{ eV} \pm 0.06 \text{ eV}$.

These parameters differ considerably from the numerous results obtained with model potentials [27] or complex-rotation-based methods [28] methods.

B. Excitation

Cross sections as a function of energy for the most important transitions from the $(2s^2)^1S$ ground state and the metastable $(2s2p)^3P^o$ excited state are presented in Figs. 3–5 for dipole, nondipole, and exchange transitions, respectively. We compare our BSR and CCC predictions with the published RMPS [6] results. For the very weak transitions, we notice some resonance-like structure near and slightly above the ionization threshold. These structures are, indeed, typical for pseudostate calculations, even if the N -electron and $(N+1)$ -electron configurations are constructed in a fully consistent manner with each other. The degree of visibility depends on the number of points displayed. Note, however, that rate coefficients involve convolution of the cross sections with the appropriate electron energy distribution function. This, together with the small values of the cross sections for which these structures appear, should ensure that there are no serious problems in collisional radiative models that employ our results. Overall, we trust that the very close agreement between several independently obtained results further

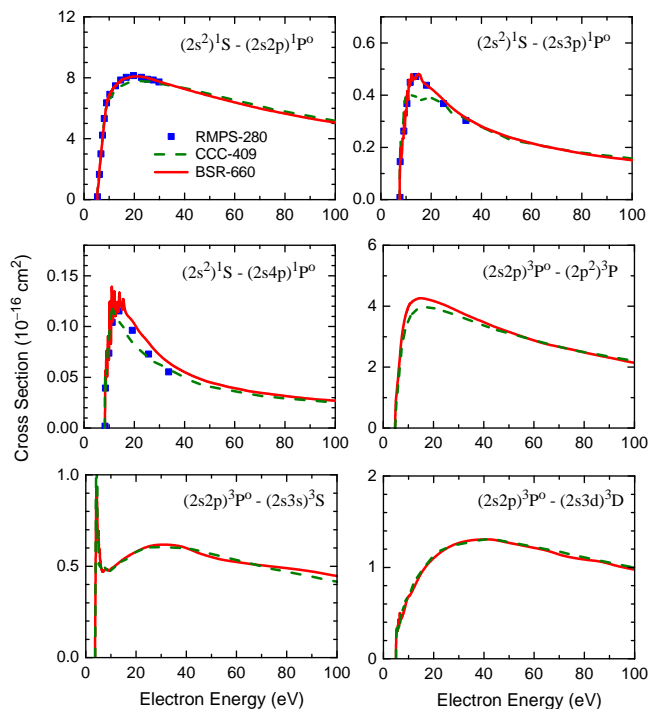


FIG. 3: (Color online) Cross sections as a function of collision energy for selected dipole transitions in beryllium. The present BSR-660 and CCC-409 results are compared with those from an earlier RMPS-280 [6] calculation.

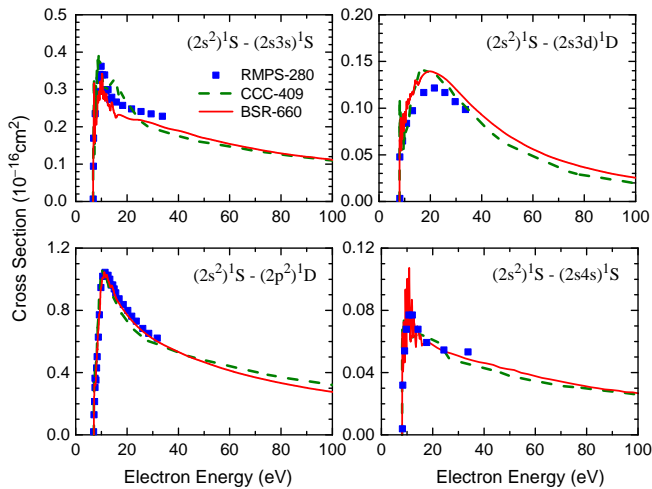


FIG. 4: (Color online) Cross sections as a function of collision energy for selected nondipole transitions in beryllium. The present BSR-660 and CCC-409 results are compared with those from an earlier RMPS-280 [6] calculation.

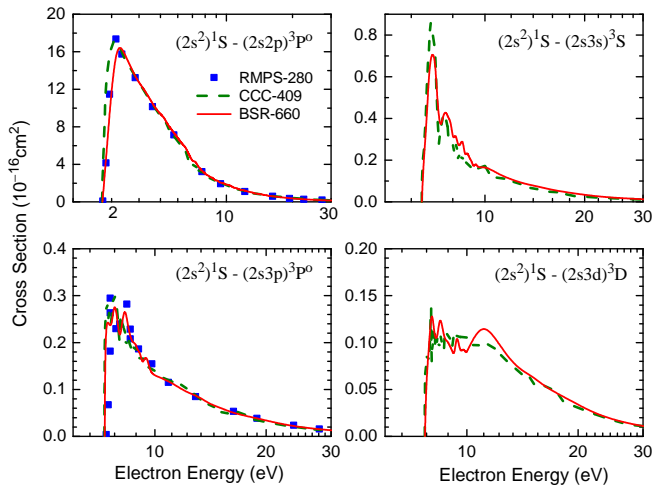


FIG. 5: (Color online) Cross sections as a function of collision energy for selected exchange transitions in beryllium. The present BSR-660 and CCC-409 results are compared with those from an earlier RMPS-280 [6] calculation.

solidifies the confidence of the plasma modeling community in using these datasets.

C. Ionization and Grand Total Cross Section

Ionization cross sections are presented in Figs. 6 and 7. The BSR-660 and CCC-409 ionization cross sections were obtained as the sum of the excitation cross section to all beryllium autoionizing states and the continuum pseudo-states. We assumed that the radiative decay of the autoionizing states is negligible in comparison to the autoionization channel. We find very good agreement between the present BSR-660 and CCC-409 results, but

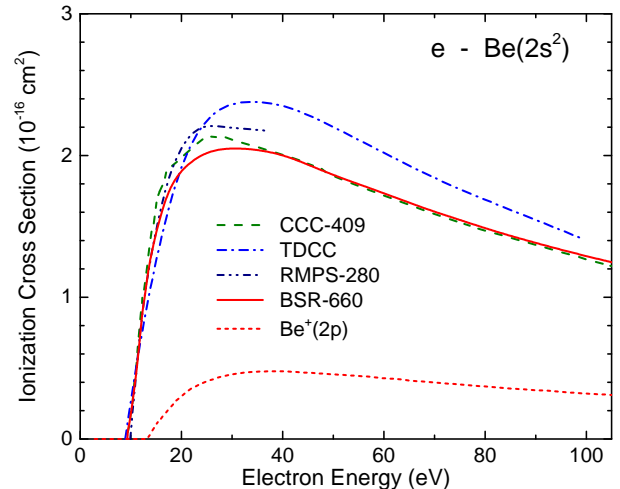


FIG. 6: (Color online) Cross section for electron-impact ionization of beryllium from the $(2s^2)^1S$ ground state. The present BSR-660 and CCC-409 results are compared with those from earlier RMPS-280 [6] and TDCC [8] calculations. Also shown is the partial cross section for producing the excited $1s^22p$ state of Be^+ (obtained with BSR-660).

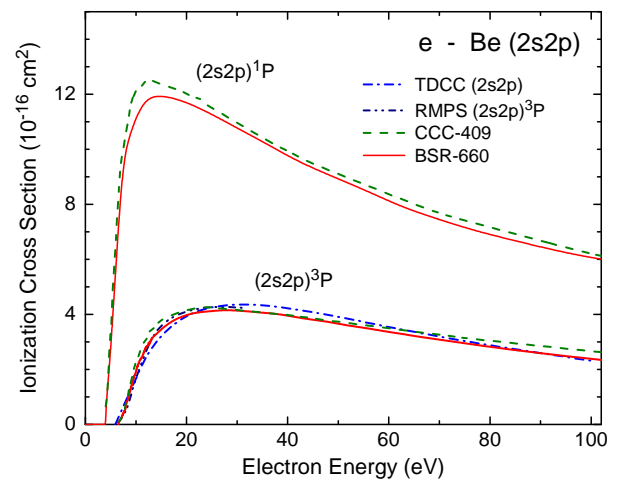


FIG. 7: (Color online) Electron-impact ionization cross sections for neutral beryllium from the first excited $2s2p$ configuration. The present BSR-660 and CCC-409 results are compared with those from earlier RMPS-280 [6] and TDCC [8] calculations.

the agreement with the earlier RMPS [6] and TDCC results [8] is also very satisfactory for ionization from both the $(2s^2)^1S$ ground state (see Fig. 6) and the metastable excited $(2s2p)^3P^o$ state (Fig. 7).

Figure 7 reveals a strong term dependence in ionization of the $(2s2p)^3P^o$ and $^1P^o$ states. This is essentially due to the well-known term dependence of the $2p$ orbital [29]. Since the TDCC model employed a $2p$ orbital that is close to the Hartree-Fock orbital optimized on the $(2s2p)^3P^o$ state, the TDCC results displayed here are expected to be most appropriate for this state.

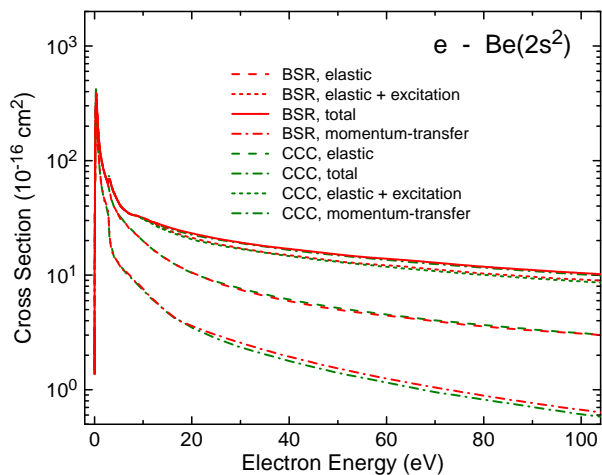


FIG. 8: (Color online) BSR-660 and CCC-409 grand total cross section for electron collisions with beryllium atoms in their $(2s^2)^1S$ ground state, along with the contributions from elastic scattering alone as well as elastic scattering plus excitation processes. Also shown is the momentum-transfer cross section.

Finally, Fig. 8 exhibits the grand total cross section for electron collisions with beryllium atoms in their $(2s^2)^1S$ ground state, i.e., the sum of angle-integrated elastic, excitation, and ionization cross sections. While the elastic cross section provides the largest contribution over the energy range shown, excitation also contributes substantially, approaching 50% for incident energies above 50 eV. Overall, ionization processes represent less than 10% of the grand total cross section. Since the momentum-transfer rather than the elastic cross section is typically important for plasma modeling, it is also shown in Fig. 8.

V. SUMMARY

We have presented an extensive set of electron scattering data for neutral beryllium, including elastic scattering, momentum transfer, excitation, and ionization processes. While state-to-state excitation cross sections were obtained for all transitions between the lowest 21 states of beryllium, results were presented for only a few selected transitions. The calculations were performed with a parallel version of the BSR code [10], in which a B -spline basis is employed to represent the continuum functions inside the R -matrix sphere. Furthermore, we utilize non-orthogonal orbitals, both in constructing the target states and in representing the scattering functions. In order to independently verify the accuracy of the BSR calculations, we also carried out CCC calculations with an

entirely different formulation of the problem and the associated computer code. Very good agreement between the BSR and CCC results was found for all calculated cross sections.

The present calculations were motivated to a large extent by the importance of accurate and thoroughly assessed e-Be collision data. For excitation as well as ionization from the ground state and the most important metastable $(2s2p)^3P$ state, we essentially confirm, where available, results from earlier RMPS [6] and TDCC [8] calculations. Furthermore, we found a significant term dependence in the ionization results for the $(2s2p)^3P$ and $(2s2p)^1P$ states, respectively.

The elastic cross section at low energies is dominated by a strong shape resonance in the $L = 1$, odd-parity channel. Since this resonance is likely of critical importance for transport processes, we carried out a systematic convergence study for its parameters. The present results, namely a position of about $0.31 \text{ eV} \pm 0.04 \text{ eV}$ above the elastic threshold with a width of $0.40 \text{ eV} \pm 0.06 \text{ eV}$, are very different from recent predictions based on a model-potential method [27] and also on a complex-rotation approach [28].

Based on our convergence studies, as well as a detailed comparison between the BSR and CCC results, we estimate the accuracy of the present dataset to be 10% or better when these data are used to obtain the relevant rate coefficients for plasma modeling applications. Electronic files with the current results, for electron energies up to 100 eV, are available from the authors upon request.

Acknowledgments

We thank Drs. B. J. Braams and H.-K. Chung for drawing our attention to the continued importance of accurate data for the e-Be collision problem, and Drs. J. Colgan and C. P. Ballance for clarifying comments on the manuscript. The work of OZ and KB was supported by the United States National Science Foundation under grants No. PHY-1212450, No. PHY-1403245, and No. PHY-1520970, and by the supercomputer allocation No. PHY-090031 within the eXtreme Science and Engineering Discovery Environment. The BSR calculations were carried out on Stampede at the Texas Advanced Computing Center and on Gordon at the San Diego Supercomputer Center. DVF and IB acknowledge support from Curtin University and resources provided by the Pawsey Supercomputing Centre with funding from the Australian Government and the Government of Western Australia.

[1] <https://www.euro-fusion.org/2013/08/beryllium-handling-facility/>

[2] <https://www.iter.org/mach/blanket>

- [3] *Light element atom, molecule and radical behaviour in the divertor and edge plasma regions (in magnetic fusion devices)*, J. Phys. Conf. Ser. **576** (2015).
- [4] *Consultancy Meeting on Evaluation and Uncertainty Assessment for Be, C, Ne Atomic Data*, Vienna (Austria, July 2015).
- [5] K. Bartschat, P. G. Burke, and M. P. Scott, J. Phys. B **30**, 5915 (1997).
- [6] C. P. Ballance, D. C. Griffin, J. Colgan, S. D. Loch, and M. S. Pindzola, Phys. Rev. A **68**, 062705 (2003).
- [7] D. V. Fursa and I. Bray, J. Phys. B **30**, 5915 (1997).
- [8] J. Colgan, S. D. Loch, M. S. Pindzola, C. P. Ballance and D. C. Griffin, Phys. Rev. A **68**, 032712 (2003).
- [9] I. Bray and D. V. Fursa, J. Phys. Conf. Ser. **576**, 012001 (2015).
- [10] O. Zatsarinny, Comp. Phys. Commun. **174** (2006) 273.
- [11] O. Zatsarinny and K. Bartschat, Phys. Rev. A **77** (2008) 062701.
- [12] O. Zatsarinny and K. Bartschat, J. Phys. B **46** (2013) 112001.
- [13] K. Bartschat and I. Bray, J. Phys. B **30** (1997) L109.
- [14] P. J. Marchalant, K. Bartschat, and I. Bray, J. Phys. B **30** (1997) L435.
- [15] J. P. Colgan, M. S. Pindzola, D. M. Mitnik, D. C. Griffin, and I. Bray, Phys. Rev. Lett. **87** (2001) 213201.
- [16] I. Bray, K. McNamara, and D. V. Fursa, Phys. Rev. A **92** (2015) 022705.
- [17] O. Zatsarinny and C. Froese Fischer, Comput. Phys. Commun. **180**, 2041 (2009).
- [18] C. Froese Fischer, Comp. Phys. Commun. **176**, 559 (2007).
- [19] A. Kramida, Yu. Ralchenko, J. Reader, and NIST ASD Team (2015). NIST Atomic Spectra Database (ver. 5.3), [Online]. Available: <http://physics.nist.gov/asd> [2016, April 28]. National Institute of Standards and Technology, Gaithersburg, MD.
- [20] A. Kramida and W. C. Martin, J. Phys. Chem. Ref. Data **26**, 1185 (1997).
- [21] G. Tachiev and C. Froese Fischer, J. Phys. B **32**, 5805 (1999).
- [22] P. G. Burke, *R-Matrix Theory of Atomic Collisions*, Springer-Verlag (Berlin, Heidelberg, 2011).
- [23] N. R. Badnell, J. Phys. B **32**, 5583 (1999); see also http://amdpp.phys.strath.ac.uk/UK_RmaX/codes.html
- [24] D. V. Fursa and I. Bray, Phys. Rev. Lett. **100**, 113201 (2008).
- [25] M. C. Zammit, D. V. Fursa and I. Bray, Phys. Rev. A **90**, 022711 (2014).
- [26] K. Bartschat, O. Zatsarinny, I. Bray, D. V. Fursa, and A. T. Stelbovics, J. Phys. B **37**, 2617 (2004).
- [27] D. Reid and J. Wadehra, J. Phys. B **47**, 225211 (2014).
- [28] T. Tsednee, L. Liang, and D. L. Yeager, Phys. Rev. A **91**, 022506 (2015).
- [29] C. Froese Fischer, *Hartree-Fock method for atoms. A numerical approach*, Wiley (New York, 1977).